5th CIRP Global Web Conference Research and Innovation for Future Production

A multi-sensor approach for fouling level assessment in clean-in-place processes

Alessandro Simeone[1], Nicholas Watson[2], Ian Sterritt[3], Elliot Woolley[1]*

[1]Centre for Sustainable Manufacturing and Recycling Technologies (SMART), Loughborough University Leicestershire, LE11 3TU, UK
[2]Faculty of Engineering, Nottingham University, UK
[3]Martec of Whitwell Ltd, Chesterfield, UK

* Corresponding author. Tel.: 4401509225410;.*E-mail address:* E.B.Woolley@lboro.ac.uk

Abstract

Clean-in-place systems are largely used in food industry for cleaning interior surfaces of equipment without disassembly. These processes currently utilise an excessive amount of resources and time, as they are based on an open loop (no feedback) control philosophy with process control dependent on conservative over estimation assumptions. This paper proposes a multi-sensor approach including a vision and acoustic system for clean-in-place monitoring, endowed with ultraviolet optical fluorescence imaging and ultrasonic acoustic sensors aimed at assessing fouling thickness within inner surfaces of vessels and pipeworks. An experimental campaign of Clean-in-place tests was carried out at laboratory scale using chocolate spread as fouling agent. During the tests digital images and ultrasonic signal specimens were acquired and processed extracting relevant features from both sensing units. These features are then inputted to an intelligent decision making support tool for the real-time assessment of fouling thickness within the clean-in-place system.

1. Introduction

In modern food manufacturing contexts, the standard procedure for cleaning equipment is the Clean-in-place (CIP) system, which uses a mix of chemicals, heat and water applied over a set period of time without the requirement of dismantling.

CIP is a multi-stage process, typically starting with a pre-rinse, followed by caustic solution wash, an intermediate rinse, and terminates with a sanitation phase made of an acid solution wash and a final rinse [1].

Existing CIP processes are time intensive and waste large amounts of energy, water, and chemicals [1,2] . Furthermore, it is estimated that on average, a food and beverage plant will spend 20% of each day on cleaning equipment, which represents significant downtime for a plant [2]. Monitoring of fouling can provide useful information on cleaning status and ensure efficient, effective operation of the equipment.

Ultraviolet (UV) light detection methods, are particularly used for the detection of residual cells and soiling on industrial surfaces [3,4]. State of the art on thickness assessment techniques includes transient thermal probe developed by [5] to estimate the fouling thickness of heat exchangers.

Pneumatic gauges for non-contact thickness measurement based on pressure profiles were developed and implemented by [6–8] presenting however distortions in measurement of soft deposit due to either the impinging jets or the suction streams [9].

An application of Heat flux sensor can be found in [10] aimed at monitoring local fouling of non-heated surfaces in commercial plants.
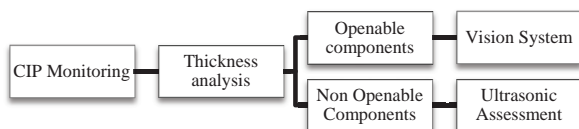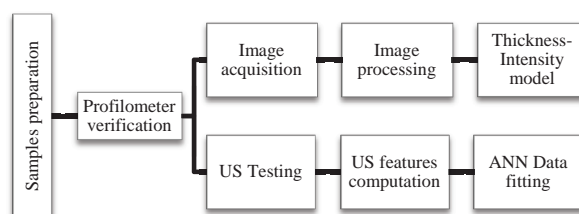
Fig. 1. Framework for thickness assessment

Fig. 2. Thickness assessment procedures

Ultrasonic (US) measurement techniques transmits low power (< 100 mW cm^{-2}) high frequency (> 20 KHz) mechanical waves through physical systems and are most commonly used is medical imaging and non-destructive testing. The techniques can be used to obtain information about the physical chemical structure of liquid materials and can identify any inhomogeneities within fluid systems by how they scatter or reflect the waves.

Ultrasound techniques have previously been used to detect fouling in heat exchangers [11–13] and pipe work [14,15]. Neural network (NN) classification can be found in [16] for determining the presence of fouling in heat exchangers.

This paper proposes a methodology for a multi-sensor monitoring system able to assess the fouling thickness within openable and non openable components of CIP equipment, utilising a vision and ultrasonic sensing units respectively for tanks and pipeworks, as outlined in Fig. 1. The output of these sensors will ultimately need to be correlated with the threshold of cleanliness to industrial standards.

2. Materials and experimental procedures

In this section, a description of the experimental setup utilised for both the vision system and ultrasonic tests is reported, with the procedure adopted for this research illustrated in Fig. 2.

2.1. Samples preparation

For the experimental campaign of thickness assessment tests, chocolate spread was used as fouling material, with the following characteristics (for 100 g of product): density=1.26 g/ml, protein = 5.4 g, water = 0 g, fat = 30 g, viscosity = 28.1 Pa·s (10 s^{-1}, 25°C).

In order to produce repeatable samples, a series of eight RK Printcoat Instruments close-wound stainless steel hand-coaters were used to apply a known-thicknesses layer of chocolate spread on two different substrate materials: stainless steel for the vision system tests and transparent polymer for ultrasonic tests.

Table 1. Nominal and measured thickness values

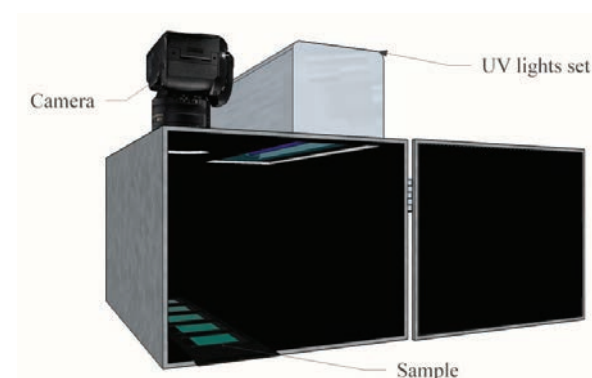| Test #	Nominal wet film deposit thickness (µm)	Measured average thickness (µm)
1	6	5.96
2	12	12.43
3	24	24.45
4	40	40.25
5	50	50.14
6	60	60.36
7	80	80.04
8	100	99.69

Fig. 3. Darkroom box design for image acquisition tests

The consistency between the sample thickness and the nominal value was verified using a Taylor Hobson CLI 2000 3D profilometer. Each sample was subject to a number of non-contact measurements, utilising the substrate as baseline and acquiring the average thickness. The nominal and measured thickness values are reported in Table 1.

2.2. Vision System setup

A darkroom box (Fig. 3) was designed and realised in order to allow a comprehensive and consistent experimental campaign of digital image acquisition of chocolate spread samples.

The darkroom box is insulated from external light sources and endowed with a set of two 18 W 370 nm fluorescent UV lights to allow the fluorescence of the chocolate layer [3].

The image acquisition was carried out using a Nikon D3300 DSLR Camera and a 10-20 mm wide angle Sigma zoom.

Nine different photographic configurations were used by varying the following parameters:
- ISO sensitivity = [1600, 3200, 6400]
- Shutter speed (s) = [1/10, 1/25, 1/50]
  Other photographic parameters were kept constant:
- Focal length = 10 mm
- F-Stop = F/5
- WB = auto

By combining the ISO sensitivity and the shutter speed values a number of 9 digital images was acquired for each test, for a total number of 72 image instances.

2.3. Ultrasonic tests setup

This research utilises a pulse echo ultrasound setup (scheme reported in Fig. 4) [17–20]. In this configuration a single ultrasound pulse is transmitted from a 2.25 MHz transducer (Imasonic IM series), reflected from the sample holder and received at the same transducer.

A Lecoeur US Box (Lecoeur Electronique, France), controlled by a laptop, is connected to the transducer and generates and receives the ultrasonic signals. The propagation of ultrasound waves are temperature dependent so the temperature within the sample cell was recorded using a PRT1000 probe and data logger (PT-104, Pico Technology Ltd, UK).

The transducer was excited by a 200 v, 7 ns flat top pulse and the received signal was amplified by 15 dB. For all experiments the sample cell was filled with water. The sample holder was removed before each measurement and the thin layer was applied on it according to the procedure described in section 2.1.

Five repetitions were carried out for each sample to increase the tests reliability, for a total number of 40 ultrasonic tests, during which, the time of flight (μm) and the received amplitude (%) data were acquired and recorded.

3. Data processing

In this section the procedures for data processing are reported, for both the vision system and the ultrasonic tests.

3.1. Vision System

The image processing procedure is illustrated in Fig. 5, and it was applied to all the 72 digital image instances.

The acquired red-green-blue (RGB) image appears as a 6000 x 4000 x 3 elements matrix, where the first two dimensions (6000 x 4000) represent the image resolution (24Mp), and the third dimension (3) represents the three colours channels red, green and blue respectively. An example of RGB image is reported in Fig. 6 for Test 8.

In order to isolate the fluorescent layer of chocolate spread from the rest of the image, the green channel was extracted from the RGB image and reported in Fig. 7. After this transformation, the green channel appears as a 6000x4000 px image in greyscale.

At this point, a manual selection of a region ofi Interest (ROI) was carried out. The ROI is identified in correspondence of the area which was previously scanned with the 3D profilometer, with a width of 20px (≈ 1 mm) and highlighted in red in Fig. 7.

The mean value of the pixel intensity was computed within the ROI for each image instance of each test for a total of 72 values.

In this way, it was possible to construct a series of thickness-intensity curves, as shown in Fig. 8. Nine curves (9 photographic conditions) of 9-point each (8 thickness samples plus the zero, assuming that thickness = 0 → intensity = 0) were plotted.
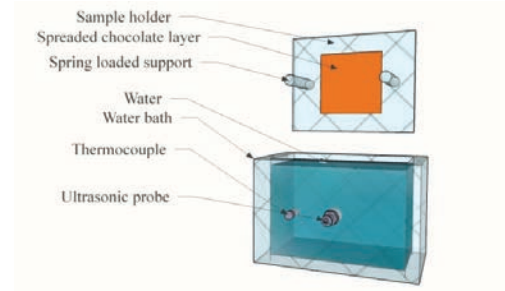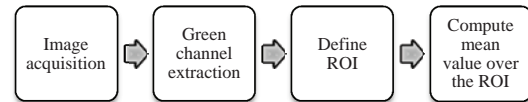

Fig. 4. Ultrasonic tests setup
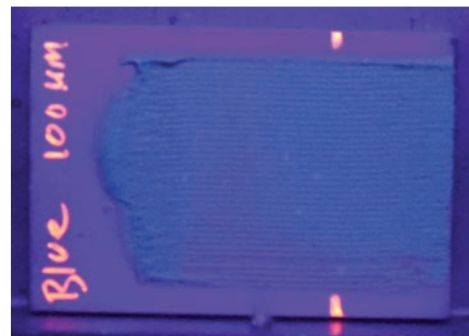

Fig. 5. Image processing flow chart

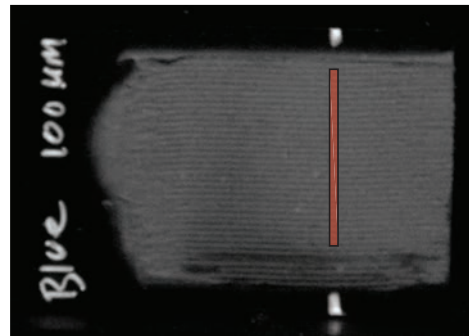Fig. 6. Test 8 (100 μm) RGB image (ISO 6400, S 1/10)

Fig. 7. Green channel image and ROI, Test 8 (ISO 6400, S 1/10)

The purpose of the image processing was to assess the thickness value given the pixel intensity; in this respect, a 3rd degree polynomial fitting was chosen to interpolate the data according to the following equation:

$$f(x) = \alpha x^3 + \beta x^2 + \gamma x + \delta$$

Where *x* is represented by the pixel intensity and *f(x)* is the computed thickness value.
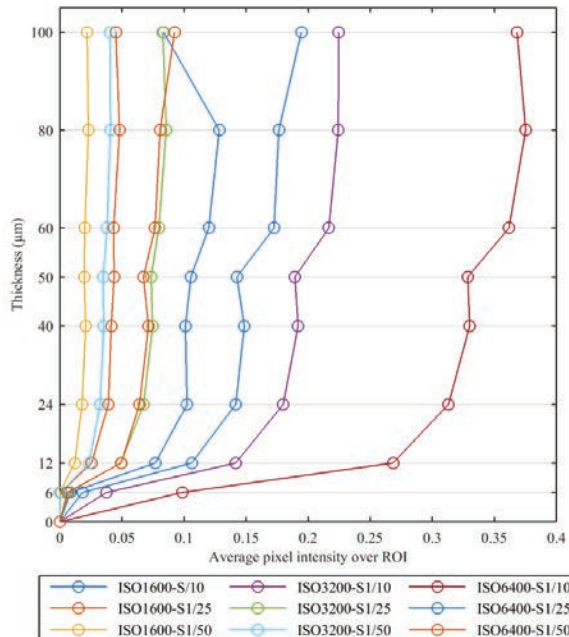
Fig. 8. Intensity-thickness curves used for polynomial fitting

This kind of fitting consists in computing the coefficient of the polynomial *f(x)* of degree 3 that fits the thickness data in a least squares sense [21].

The data fitting procedure was applied to all the nine curves and the table of coefficients [α β γ δ] is reported in Table 2 for all the photographic configurations. Outliers were removed from the curve fitting modelling.

3.2. Ultrasonic signal processing

US data were processed in order to compute the-Ultrasonic path length, which was calculated by multiplying the ultrasonic velocity through the water by the Time of Flight of the received signal.

The Time of Flight was recorded as the first zero crossing once the received signal is larger than the selected threshold value. To account for temperature effects the ultrasonic velocity is calculated using the Marczak Equation reported below [22].

$$c = 1.402385 \times 10^3 + 5.038813\,T - 5.799136 \times 10^{-2}\,T^2 + 3.287156 \times 10^{-4}\,T^3 - 1.398845 \times 10^{-6}\,T^4 + 2.787860 \times 10^{-9}\,T^5$$

Where T is the water temperature measured using the embedded thermocouple (°C).

The received signal amplitude is a function of attenuation through the propagating fluid and the percentage of reflected signal from the sample holder (with or without fouling layer).

The percentage of reflected signal depends on the relative acoustic impedance (z) of the water and reflecting surface: $z = \rho c$, where c is the ultrasonic velocity and ρ the density of each material [23].

Table 2. Polynomial coefficients

Configuration	α	β	γ	δ
ISO1600-S1/10	7.71E+04	-7143	254.6	1.846
ISO1600-S1/25	3.85E+06	-2.14E+05	3314	0.1667
ISO1600-S1/50	2.62E+07	-6.24E+05	4347	2.886
ISO3200-S1/10	2.63E+04	-5927	387.4	-0.535
ISO3200-S1/25	6.23E+05	-5.99E+04	1653	-1.16
ISO3200-S1/50	7.30E+06	-3.68E+05	5074	1.378
ISO6400-S1/10	5148	-1815	174.9	0.3628
ISO6400-S1/25	2.42E+04	-2857	154.7	1.574
ISO6400-S1/50	2.05E+05	-1.48E+04	716.7	0.9556

Table 3. 2-element ultrasonic feature vector

ID Test	US path length (mm)	Received amplitude (%)
T 1.1	38.1941	33
T 1.2	38.3098	34
…	…	…
T 8.4	38.0093	10
T 8.5	38.0043	11

A large acoustic impedance difference results in a larger proportion of the signal been reflected. There is the potential for signal attenuation (due to acoustic absorption, weak reflections, depth of penetration, etc.) to create a problem in terms of signal-to-noise ratios, but this was not observed in this study. Any such problems could be overcome by using multiple ultrasonic detection methods.

4. Neural network data fitting for thickness assessment

Ultrasonic features, i.e. *US Path* and *Amplitude* were grouped in a 2-element feature vector [24] (partially reported in Table 3) and inputted to a Neural Network data fitting [25] decision making support system for thickness assessment purpose.

Three-layer feed-forward neural networks were built with the following architecture:

- Input layer: 2 nodes corresponding to the US feature vector (40 instances x 2 features)
- Hidden layer nodes (HLN): variable
- Target layer: 1 node corresponding to the nominal thickness value (6, 12, 24, 40, 50, 60, 80, 100 μm) of each instance (40 instances x 1 thickness value)

Several NN configuration were considered, by varying the number of hidden layer nodes: 4, 8 and 16, and the training algorithm, i.e. Levenberg-Marquardt (LM) [26], Bayesian regularisation (BR) [27,28] and scaled conjugate gradient (SCG) [29]. Data division for NN learning was carried out randomly with the following percentages: 70% for training, 15% for validation and 15% for testing [29].

5. Results and discussions

In this section the results of the vision system and ultrasonic experimental tests are presented and discussed.

5.1. Vision System

Considering the polynomial fitting model computed for a given set of photographic conditions, it is possible to build a 3D mesh plot of the surface fouling within an openable component (see Fig. 9), where the x- and y-axes represent the image resolution, and the z-axis represents the computed fouling thickness. It should be noted that image acquisition and processing for fouling assessment is applied in a time-lapse context of fouling monitoring within openable components of CIP systems. In this way it is possible to have a real-time assessment of the fouling within the tank and its removal rate in order to adapt, during the cleaning process, the cleaning parameters such as time, detergent concentration and potentially water pressure and water spray direction.

5.2. Ultrasonic tests

The goodness of fitting is shown in terms of Pearson Correlation Coefficient R, defined as [30]:

$$R = \frac{\sum_{i=1}^{n}(x_i - \bar{x})(y_i - \bar{y})}{\sqrt{\sum_{i=1}^{n}(x_i - \bar{x})^2 \sum_{i=1}^{n}(y_i - \bar{y})^2}}$$

Where x is the target vector (nominal thickness values) and y is the estimated thickness value. The coefficients were calculated for all the stages of the NN fitting: training, validation, testing and a total one. A synoptic chart of the overall R coefficients vs hidden layer nodes and training algorithm is reported in Fig. 10.

All the NN configurations adopted yielded to a Correlation coefficient higher than 0.9 which demonstrates a good suitability of the US features in assessing the fouling thickness.

For this specific application, the best fitting is given by LM-4HLN NN configuration, which corresponds to the Levenberg-Marquardt training algorithm with 4 hidden layer nodes. A detailed regression plot for this configuration is reported in Fig. 11 including training, validation, testing and total regressions. The number of hidden layer nodes doesn't show a clear influence on results trend, whilst, on average, the most consistent training algorithm results to be the BR.
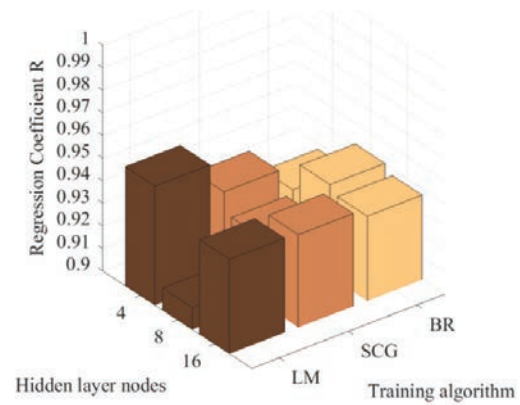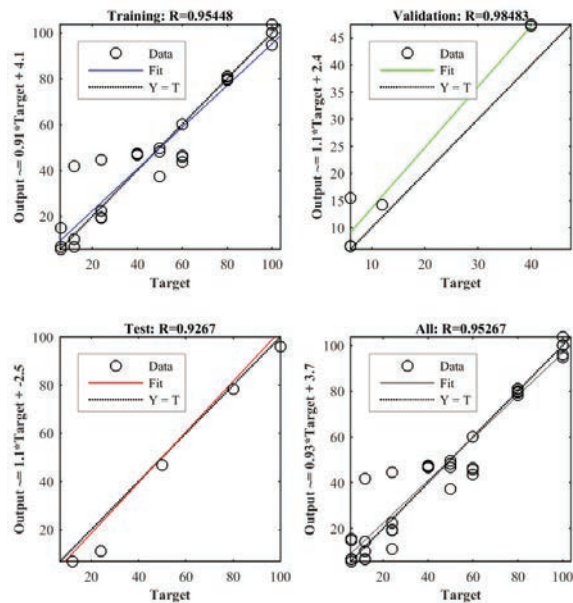

Fig. 10. Data Fitting Results

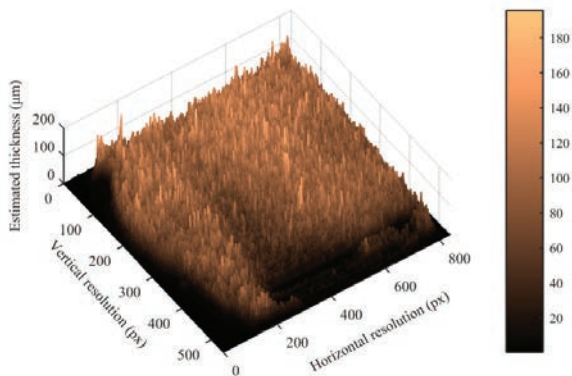Fig. 11. Regression plots for the LM-4HLN configuration

6. Conclusions

For a comprehensive clean-in-place monitoring system a broad study on the thickness assessment needs to be carried out. In this paper two methodologies were proposed, for openable components and non openable components respectively.

A vision system endowed with UV light was set up to model the fouling thickness within tanks and vessels, and an ultrasonic intelligent system was used to assess the fouling thickness within pipeworks.

A correlation between the fouling thickness and the pixel intensity was found, enabling a real time control of the fouling removal rate.

Ultrasonic tests results indicated that the technique was capable of determining the thickness of the fouling material in

Fig. 9. 3D mesh plot of thickness, Test 8 (ISO 6400 S 1/10)

real-time with a similar level of sensitivity as the vision technique.

Future work will include the implementation on a laboratory scale CIP system featuring a range of typical process operating conditions and fouling materials. This work will combine the two sensor techniques demonstrated in the current work into a system capable of characterising the internal surface fouling conditions within different components simultaneously to deliver real-time data on cleaning performance.

Moreover, further investigation needs to be carried out on the correlation between the sensor monitoring system outputs and Adenosine Triphosphate (ATP) swabbing technique. This standard is currently utilised within the food and drink industry to determine the cleanliness level. This will enable the real-time monitoring of the fouling removal which is suitable for industrial applications.

Acknowledgements

References

1. Thomas A, Sathian CT. Cleaning-In-Place (CIP) System in Dairy Plant-Review. IOSR J Environ Sci Ver III [Internet]. 2014;8(6):2319–99. Available from: www.iosrjournals.org
2. Jude B, Lemaire E. How to Optimize Clean-in-Place (CIP) Processes in Food and Beverage Operations [Internet]. Schneider Electric White Paper. 2013. Available from: http://www2.schneider-electric.com/documents/support/white-papers/energy-efficiency/how-to-optimize-clear-in-place-CIP-processes.pdf
3. Whitehead K a., Smith L a., Verran J. The detection of food soils and cells on stainless steel using industrial methods: UV illumination and ATP bioluminescence. Int J Food Microbiol. 2008;127(1-2):121–8.
4. Ichimura M, Nam S, Bonjour S, Rankine H, Carisma B, Qiu Y, et al. Eco-efficiency Indicators: Measuring Resource-use Efficiency and the Impact of Economic Activities on the Environment [Internet]. "Greening of economic growth" series. 2009. Available from: https://sustainabledevelopment.un.org/content/documents/785eco.pdf
5. Perez L, Ladevie B, Tochon P, Batsale JC. A new transient thermal fouling probe for cross flow tubular heat exchangers. Int J Heat Mass Transf. 2009;52(1-2):407–14.
6. Gale GE. A thickness measuring device using pneumatic gauging to detect the sample. Meas Sci Technol [Internet]. 1995;6(11):1566. Available from: http://stacks.iop.org/0957-0233/6/i=11/a=003
7. Changani SD, Belmar-Beiny MT, Fryer PJ. Engineering and chemical factors associated with fouling and cleaning in milk processing. Exp Therm Fluid Sci. 1997;14(4):392–406.
8. Tuladhar, T.R., Paterson, W.R., Macleod, N. and Wilson DI. Development of a Novel Non-Contact Proximity Gauge for Thickness Measurement of Soft Deposits and its Application in Fouling Studies. Can J Chem Eng. 2000;78(October):935–47.
9. Lee SS, Chen JC. On-line surface roughness recognition system using artificial neural networks system in turning operations. Int J Adv Manuf Technol [Internet]. 2003 Nov 1 [cited 2015 Jul 10];22(7-8):498–509. Available from: http://link.springer.com/10.1007/s00170-002-1511-z
10. Truong T, Anema S, Kirkpatrick K, Chen H. The Use of a Heat Flux Sensor for In-Line Monitoring of Fouling of Non-Heated Surfaces. Food Bioprod Process [Internet]. 2002;80(4):260–9. Available from: http://www.sciencedirect.com/science/article/pii/S0960308502703313
11. Withers P. Ultrasonic sensor for the detection of fouling in UHT processing plants. Food Control. 1994;5(2):67–72.
12. Withers PM. Ultrasonic, acoustic and optical techniques for the non-invasive detection of fouling in food processing equipment. Vol. 7, Trends in Food Science and Technology. 1996. p. 293–8.
13. Lohr KR, Rose JL. Ultrasonic guided wave and acoustic impact methods for pipe fouling detection. J Food Eng. 2003;56(4):315–24.
14. Merheb B, Nassar G, Nongaillard B, Delaplace G, Leuliet JC. Design and performance of a low-frequency non-intrusive acoustic technique for monitoring fouling in plate heat exchangers. J Food Eng. 2007;82(4):518–27.
15. Wallhäußer E, Hussein WB, Hussein MA, Hinrichs J, Becker TM. On the usage of acoustic properties combined with an artificial neural network--A new approach of determining presence of dairy fouling. J Food Eng. 2011;103(4):449–56.
16. Wallhäußer E, Sayed A, Nöbel S, Hussein M a., Hinrichs J, Becker T. Determination of cleaning end of dairy protein fouling using an online system combining ultrasonic and classification methods. Food Bioprocess Technol. 2013;7:506–15.
17. Blitz J, Simpson G. Ultrasonic methods of non-destructive testing. Vol. 2. Springer Science & Business Media; 1995.
18. Segreto T, Bottillo A, Teti R. Advanced Ultrasonic Non-destructive Evaluation for Metrological Analysis and Quality Assessment of Impact Damaged Non-crimp Fabric Composites. Procedia CIRP [Internet]. 2016;41:1055–60. Available from: http://www.sciencedirect.com/science/article/pii/S2212827115012044
19. Shull PJ. Nondestructive evaluation: theory, techniques, and applications. CRC press; 2002.
20. Povey MJW. Ultrasonic techniques for fluids characterization. Academic Press; 1997.
21. Chernov N, Ma H. Least squares fitting of quadratic curves and surfaces. Comput Vis. 2011;285–302.
22. Marczak W. Water as a standard in the measurements of speed of sound in liquids. J Acoust Soc Am. 1997;102(April 1996):2776.
23. Kinsler LE, Frey AR, Coppens AB, Sanders J V. Fundamentals of acoustics. Vol. 1, Fundamentals of Acoustics, 4th Edition, by Lawrence E. Kinsler, Austin R. Frey, Alan B. Coppens, James V. Sanders, pp. 560. ISBN 0-471-84789-5. Wiley-VCH, December 1999. 1999. p. 560.
24. Segreto T, Simeone A, Teti R. Principal component analysis for feature extraction and NN pattern recognition in sensor monitoring of chip form during turning. CIRP J Manuf Sci Technol. 2014;7(3):202–9.
25. Maghsoudi M, Ghaedi M, Zinali A, Ghaedi AM, Habibi MH. Artificial neural network (ANN) method for modeling of sunset yellow dye adsorption using zinc oxide nanorods loaded on activated carbon: Kinetic and isotherm study. Spectrochim Acta - Part A Mol Biomol Spectrosc. 2015;134:1–9.
26. Marquardt DW. An Algorithm for Least Squares Estimation of Nonlinear Parameters. J Soc Ind Appl Math. 1963;11(2):431–41.
27. MacKay DJC. Bayesian Interpolation. Neural Comput. 1992;4(3):415–47.
28. Foresee FD, Hagan MT. Gauss-Newton approximation to Bayesian regularization. Proc 1997 Int Jt Conf Neural Networks. 1997;1930–5.
29. Moller M. A scaled conjugate gradient algorithm for fast supervised learning. Neural Networks [Internet]. 1993;6:525–33. Available from: http://linkinghub.elsevier.com/retrieve/pii/S0893608005800565
30. Asuero a. G, Sayago A, González a. G. The Correlation Coefficient: An Overview. Crit Rev Anal Chem. 2006;36:41–59.